

Article

# Antifragility Predicts the Robustness and Evolvability of Biological Networks through Multi-Class Classification with a Convolutional Neural Network

Hyobin Kim <sup>1,2</sup> , Stalin Muñoz <sup>3</sup> , Pamela Osuna <sup>4</sup> and Carlos Gershenson <sup>5,6,7,\*</sup> 

<sup>1</sup> Biotech Research and Innovation Centre (BRIC), University of Copenhagen (UCPH), 2200 Copenhagen, Denmark; hyobin.kim@c3.unam.mx

<sup>2</sup> Novo Nordisk Foundation Center for Stem Cell Biology, DanStem, Faculty of Health Sciences, University of Copenhagen, 2200 Copenhagen, Denmark

<sup>3</sup> Institute for Software Technology (IST), Graz University of Technology, 8010 Graz, Austria; stalin.munoz@c3.unam.mx

<sup>4</sup> Faculté des Sciences et Ingénierie, Sorbonne Université, 75005 Paris, France; ana.osuna\_vargas@etu.upmc.fr

<sup>5</sup> Centro de Ciencias de la Complejidad, Universidad Nacional Autónoma de México, CDMX 04510, Mexico

<sup>6</sup> Instituto de Investigaciones en Matemáticas Aplicadas y en Sistemas, Universidad Nacional Autónoma de México, CDMX 04510, Mexico

<sup>7</sup> Department of High Performance Computing, ITMO University, 199034 St. Petersburg, Russia

\* Correspondence: cgg@unam.mx

Received: 10 August 2020; Accepted: 2 September 2020; Published: 4 September 2020



**Abstract:** Robustness and evolvability are essential properties to the evolution of biological networks. To determine if a biological network is robust and/or evolvable, it is required to compare its functions before and after mutations. However, this sometimes takes a high computational cost as the network size grows. Here, we develop a predictive method to estimate the robustness and evolvability of biological networks without an explicit comparison of functions. We measure antifragility in Boolean network models of biological systems and use this as the predictor. Antifragility occurs when a system benefits from external perturbations. By means of the differences of antifragility between the original and mutated biological networks, we train a convolutional neural network (CNN) and test it to classify the properties of robustness and evolvability. We found that our CNN model successfully classified the properties. Thus, we conclude that our antifragility measure can be used as a predictor of the robustness and evolvability of biological networks.

**Keywords:** robustness; evolvability; antifragility; complexity; prediction; Boolean networks; gene regulatory networks; convolutional neural networks

## 1. Introduction

Robustness and evolvability are prevalent in the evolution of biological systems [1–6]. As studying the relationship between the two properties is necessary for understanding how biological systems can withstand mutations and simultaneously generate genetic variations, numerous studies on their relationship have been done [7–11]. Robustness allows the existing functions to be preserved in the presence of mutations or perturbations, while evolvability enables new functions to be expressed for adapting to new environments [12–14]. To determine if a biological system is robust and/or evolvable, the comparison of its functions before and after internal perturbations is needed. Pragmatically, in Boolean networks used as gene regulatory network models, the definition of robust and evolvable networks has been established via the comparison of dynamic attractors (i.e., stable steady states) before and after internal perturbations [14] based on numerical and experimental evidence showing that the attractors represent cell types or cell functions [15–17].

The definition of robustness and evolvability has been applied to a number of studies adopting Boolean network models in artificial life and systems biology [18–20]. However, the calculations for finding all attractors of the networks are computationally expensive. This is because as the network size  $N$  grows, there is a combinatorial explosion of the state space (i.e., the set of all possible states, whose size is  $2^N$ ). As an alternative to this exhaustive approach, some studies where large networks are explored only sample the state space. This implies that only the attractors with the largest basins (i.e., the sets of states leading to attractors) are found [14,19,21]. However, in the case of extremely long attractor lengths, many number of attractors, and/or evenly distributed basins of attraction, this strategy will give biased results. Here, we aim to develop a predictor of robustness and evolvability without the explicit comparison of the functions (i.e., attractors), and thus applicable to large networks.

We use antifragility to estimate the robustness and evolvability of biological networks. Antifragility can be defined as the ability of a system to improve its functionality in the presence of external perturbations [22]. In the context of Boolean networks, it can be measured by our previous approach [23,24], where antifragility is easily calculated by means of complexity computed from partial state transitions. With the differences of antifragility before and after internal perturbations, we train a CNN model and then test it to classify the properties of robustness and evolvability. We found that our model successfully classified both properties. Thus, we conclude that antifragility can be used as a significant predictor of robustness and evolvability.

Our predictor—antifragility—has many potential applications. It would be useful to systems and computational biologists studying the properties of large biological networks from a dynamical perspective. They could find out if the large networks have the potential of being either robust or evolvable, or both without investigating how the functions (attractors) of the networks are changed before and after mutations. Moreover, understanding antifragility would be helpful for uncovering the mechanism of how biological systems acquired robustness and evolvability. In addition, our antifragility measure could be used as a control parameter to build robust and/or evolvable engineered systems.

## 2. Materials and Methods

### 2.1. Boolean Networks and Biological Systems

Boolean networks were proposed by Stuart Kauffman as gene regulatory network models [25–27]. They have been extensively used in many areas including artificial life, robotics, and systems biology [28–34]. They consist of nodes and links, where nodes represent genes, and the links represent interactions between genes. Each node has a binary state 0 (OFF) or 1 (ON). Zero means being inhibited, and 1 indicates being activated or expressed. The future state of each node is determined by a lookup table. The states of nodes are updated synchronously in discrete time. Once the network topology and the lookup tables for each node are set, they remain fixed.

If the links are randomly arranged, and the node states are updated by Boolean functions randomly assigned to each node, the networks are called random Boolean networks (RBNs). RBNs are also known as Kauffman's  $NK$  Boolean networks, where  $N$  is the number of nodes and  $K$  is the number of links per node (self-links can be included). Meanwhile, the links and the update rules of Boolean network models of biological systems are determined by experiments and literature that have identified actual relationships between genes (or proteins).

In Figure 1, an example RBN and its state transition diagram are presented. With a Boolean network with  $N$  nodes, its state transition diagram graphically represents  $2^N$  states and transitions among them. In the state transition diagram, there are two important concepts: One is attractors, and the other is basins of attraction. Attractors are states in a fixed-point or a limit cycle, and basins of attraction are the rest of the configurations going toward attractors. For a better understanding, we provide formal definitions of a Boolean network, an attractor, and a basin of attraction as follows [35]:

- We denote a Boolean network as  $G(V, F)$  composed of a set  $V = \{v_1, v_2, \dots, v_N\}$  of nodes and a list  $F = (f_1, f_2, \dots, f_N)$  of Boolean functions, in which  $f_i(v_{i_1}, v_{i_2}, \dots, v_{i_k})$  is the Boolean function

assigned to node  $v_i$  and has input nodes  $v_{i_1}, v_{i_2}, \dots, v_{i_k}$ .  $IN(v_i)$  signifies the set of input nodes  $v_{i_1}, v_{i_2}, \dots, v_{i_k}$  to  $v_i$ .

- The state of each node is 0 or 1 at discrete time  $t$ . We use  $v_i(t)$  to indicate the state of node  $v_i$  at time  $t$ . Then, the state of node  $v_i$  at time  $t + 1$  is denoted by  $v_i(t + 1) = f_i(v_{i_1}(t), v_{i_2}(t), \dots, v_{i_k}(t))$ .
- If we designate  $[v_1(t), v_2(t), \dots, v_N(t)]$  as  $v(t)$ ,  $v_i(t + 1)$  is simply written by  $v_i(t + 1) = f_i(v(t))$ .  $v(t)$  means a gene expression profile at time  $t$ . For the whole Boolean network, it is written by  $v(t + 1) = f(v(t))$ .
- The set of edges  $E$  is defined as  $E = \{(v_{i_j}, v_i) | v_{i_j} \in IN(v_i)\}$ . Then,  $G(V, E)$  represents a directed graph which shows the network topology. An edge from  $v_{i_j}$  to  $v_i$  means that  $v_{i_j}$  has an effect on the expression of  $v_i$ .  $K$  is the in-degree of  $v_i$ .
- An initial  $v(0)$  eventually converges into a set of state configurations, which is defined as an attractor. When an attractor is composed of only one state configuration (i.e.,  $v = f(v)$ ), it is a fixed-point attractor. When an attractor is composed of more than one state configuration, it is a cyclic attractor with period  $l$  if it consists of  $l$  state configurations (i.e.,  $v^1 = f(v^l) = f(f(v^{l-1})) = \dots = f(f(\dots f(v^1)\dots))$ ). Here,  $l$  is called attractor length. The set of state configurations which eventually reach the same attractor is defined as basin of attraction. For example, in Figure 1, 000, 010, and 111 are fixed-point attractors. {011, 110} is a cyclic attractor with  $l = 2$ . {100, 101} belongs to the basin of the cyclic attractor {011, 110}.

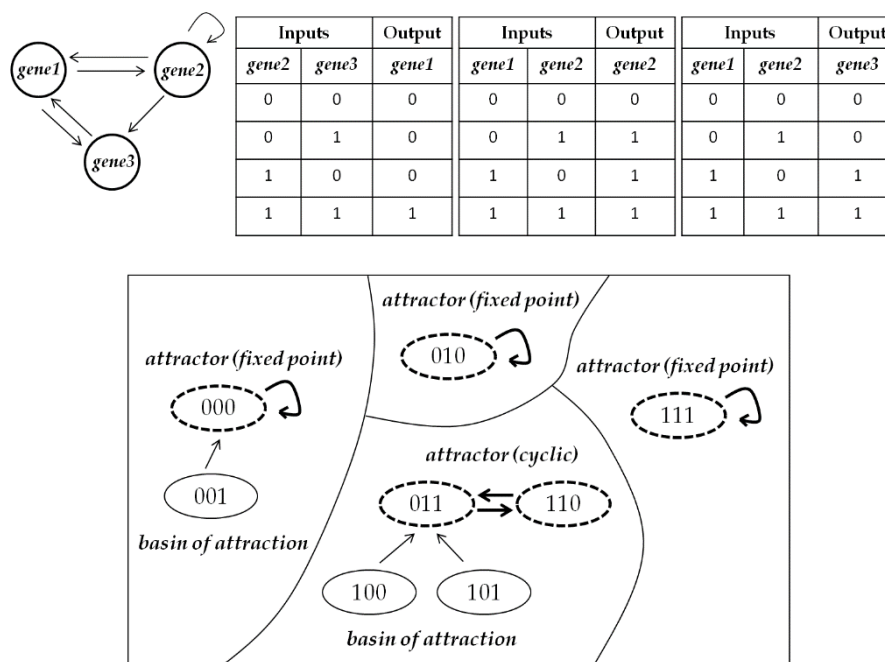


**Figure 1.** An example random Boolean network (RBN) with  $N = 3$  and  $K = 2$  and its state transition diagram. The topology is randomly generated and Boolean functions are randomly assigned to each node. The state transition diagram is composed of  $2^3 = 8$  state configurations from 000 to 111 and transitions among them. In the state transition diagram, attractors are the configurations with bold dashed lines, and basins of attraction are the configurations except for the attractors.

In this study, we use different Boolean network models of 37 biological systems. The range of the network size is from 5 to 26. We find all attractors and basins of attraction by exhaustively tracking which states all state configurations finally converge to. Therefore, to find the attractors and basins for the ten thousand networks within a reasonable time, 26 nodes ( $2^{26} = 67,108,864$  states) are the maximum network size we can handle in our computing environment. Table 1 shows information

about the biological networks collected from the Cell Collective public platform for modeling biological networks. In the table, the networks are sorted by their size.

**Table 1.** Different Boolean network models of 37 biological systems used for simulations.

Biological Network <sup>1</sup>	No. of Nodes	No. of Links	Ref.
#1. Cortical area development (cortical)	5	14	[36]
#2. Cell cycle transcription by coupled CDK and network oscillators (cycle-cdk)	9	19	[37]
#3. Mammalian cell cycle (core-cell-cycle)	10	35	[38]
#4. Toll pathway of drosophila signaling pathway (toll-drosophila)	11	11	[39]
#5. Metabolic interactions in the gut microbiome (metabolic)	12	30	[40]
#6. Regulation of the L-arabinose operon of Escherichia coli (l-arabinose-operon)	13	18	[41]
#7. Lac operon (lac-operon-bistability)	13	22	[42]
#8. Arabidopsis thaliana cell-cycle (arabidopsis)	14	66	[43]
#9. Fanconi anemia and checkpoint recovery (anemia)	15	66	[44]
#10. Cardiac development (cardiac)	15	38	[45]
#11. BT474 breast cell line short-term ErbB network (bt474-ErbB)	16	46	[44,46]
#12. SKBR3 breast cell line short-term ErbB network (skbr3-short)	16	41	[46]
#13. Neurotransmitter signaling pathway (neurotransmitter)	16	22	[47]
#14. HCC1954 breast cell line short-term ErbB network (hcc1954-ErbB)	16	46	[46]
#15. Body segmentation in drosophila (body-drosophila)	17	29	[48]
#16. CD4+ T cell differentiation and plasticity (cd4)	18	78	[49]
#17. Budding yeast cell cycle (budding-yeast)	18	59	[50]
#18. T-LGL survival network (t-lgl-survival)	18	43	[51]
#19. VEGF pathway of drosophila signaling pathway (vegf-drosophila)	18	18	[39]
#20. Oxidative stress pathway (oxidative-stress)	19	32	[49,52]
#21. Human gonadal sex determination (gonadal)	19	79	[53]
#22. Mammalian cell-cycle (mammalian)	20	51	[52,54]
#23. Budding yeast cell cycle (yeast-cycle)	20	42	[55]
#24. B cell differentiation (b-cell)	22	39	[56]
#25. Iron acquisition and oxidative stress response in aspergillus fumigatus (aspergillus-fumigatus)	22	38	[57]
#26. FGF pathway of drosophila signaling pathways (fgf-drosophila)	23	24	[39]
#27. T cell differentiation (t-cell-differentiation)	23	34	[58]
#28. Aurora kinase A in neuroblastoma (aurka)	23	43	[59]
#29. Processing of Spz Network from the drosophila signaling pathway (spz-drosophila)	24	28	[39]
#30. TOL regulatory network (tol)	24	48	[60]
#31. HH pathway of drosophila signaling pathways (hh-drosophila)	24	32	[39]
#32. HCC1954 breast cell line long-term ErbB network (hcc1954)	25	70	[46]
#33. SKBR3 breast cell line long-term ErbB network (skbr3-long)	25	81	[46]
#34. BT474 breast cell line long-term ErbB network (bt474)	25	70	[46]
#35. Wg pathway of drosophila signaling pathways (wg-drosophila)	26	29	[39]
#36. Trichostrongylus retortaeformis (trichostrongylus)	26	58	[61]
#37. Pro-inflammatory tumor microenvironment in acute lymphoblastic leukemia (leukemia)	26	81	[62]

<sup>1</sup> Data was obtained from Cell Collective (<https://research.cellcollective.org/?dashboard=true#>).

## 2.2. Mutations and Classification of Robustness and Evolvability

We introduce four types of random mutations to each biological network to study their robustness and evolvability: We add, delete one regulatory link, change the position of a link in the network, or flip one state (i.e., 0 changes into 1, and 1 changes into 0) in the output of Boolean functions assigned to each node [63–65]. These four types of mutations are distributed as equally as possible. Then, we measure properties of different mutants without repetitions and compare them with the original networks.

Comparing the attractors between the original and mutated networks, we classify the properties of biological networks [66]. Our classification is extended from the definition of robust and evolvable network in Aldana et al.'s work [14]. They added perturbations to a network structure and then

observed attractors between the original and perturbed networks. Under the assumption that all attractors represent essential cell types or cell functions, they considered the preservation of attractors robustness and the emergence of new attractors evolvability.

Based on their concept, we divide the properties of robustness and evolvability into four classes: Not robust & not evolvable, not robust & evolvable, robust & not evolvable, and robust & evolvable (Figure 2). For example, an original network has a set of attractors  $A = \{a_1, a_2, a_3\}$ .

- Not robust & not evolvable: The mutated network does not have exactly the same attractors as the attractors of the original network and further does not produce any new attractors. It is the case where the mutated network has a set of attractors  $A' = \{a_1, a_2\}$  ( $A \supset A'$ ).
- Not robust & evolvable: The mutated network does not fully have original attractors but creates new attractors. It is the case where the mutated network has a set of attractors  $A' = \{a_1, a_4\}$  ( $A \neq A'$  and  $AA'$  and  $A'A$ ).
- Robust & not evolvable: The mutated network maintains the original attractors but does not generate any new attractors. It is the case where the mutated network has a set of attractors  $A' = \{a_1, a_2, a_3\}$  ( $A = A'$ ).
- Robust & evolvable: The mutated network has the same attractors as the original one and simultaneously produces new attractors. It is the case where the mutated network has a set of attractors  $A' = \{a_1, a_2, a_3, a_4, a_5\}$  ( $A \subset A'$ ).

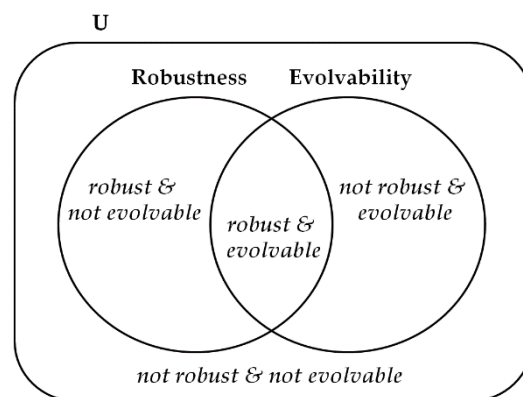


**Figure 2.** The schematic diagram of the four classes on robustness and evolvability. Depending on the change of attractors between original and mutated networks, the network is certainly classified into one class among not robust & not evolvable, not robust & evolvable, robust & not evolvable, and robust & evolvable.

In our simulations, we independently add an internal perturbation 1000 times to each network, and then get 1000 perturbed networks per biological network. Next, we classify the properties of all the perturbed networks into the above four classes. Since one biological network can be not robust & not evolvable, not robust & evolvable, robust & not evolvable, or robust & evolvable against the 1000 perturbations, we can get the percentage frequency distribution of the four classes per network.

### 2.3. Antifragility in Boolean Networks

Antifragility was defined by Taleb [22]. Antifragility is the property of a system that improves when exposed to perturbations. We recently developed a measure to assess antifragility in Boolean networks [23,24]. In this study, we employed this antifragility measure. One advantage of this measure is that its computation time increases linearly with  $N$  (Figure S2 in Supplementary Material).

On the assumption that antifragility indicating responses to external perturbations might be helpful to predict responses to internal perturbations (i.e., mutations), we use antifragility as a predictor to estimate the robustness and evolvability of biological networks against mutations. To understand our antifragility measure, we first have to explain how we measure complexity and external perturbations.

### 2.3.1. Complexity of Boolean Networks

Complexity can be seen as a balance between change and regularity [26]. In terms of information, change means that information becomes different, while regularity means that information is preserved. In biology, a balance between the change and preservation of genetic information enables biological systems to have flexibility and stability by which biological systems robustly adapt to their environment.

We defined the change and regularity as emergence and self-organization, respectively and developed measures to quantify them. Moreover, using the two metrics, we presented a measure to evaluate complexity [67,68]. Complexity ( $C$ ) is calculated from emergence ( $E$ ) and self-organization ( $S$ ) as follows:

$$C = 4 \times E \times S \tag{1}$$

where coefficient 4 is added to normalize the values of  $C$  to the range of  $[0,1]$  ( $0 \leq C \leq 1$ ). Since  $S$  can be regarded as the complement of  $E$  [67,68], Equation (1) is reformulated by the following equation:

$$C = 4 \times E \times (1 - E) \tag{2}$$

In a Boolean network which consists of  $N$  nodes,  $E$  ( $0 \leq E \leq 1$ ) is measured as the average of emergence values for all nodes, where the emergence of each node is computed through Shannon’s information entropy:

$$E = \frac{\sum_{i=1}^N E_i}{N} = \frac{\sum_{i=1}^N -(p_0^{(i)} \log_2 p_0^{(i)} + p_1^{(i)} \log_2 p_1^{(i)})}{N} \tag{3}$$

where  $p_0^{(i)}$  ( $p_1^{(i)}$ ) is the ratio of how many 0 s (1 s) are expressed to  $T$  state transitions for node  $i$  (i.e.,  $p_0^{(i)} + p_1^{(i)} = 1$ ). Regarding  $T$ , we obtain  $p_0^{(i)}$  ( $p_1^{(i)}$ ) on state transitions not from 1 to  $T$  but from  $T + 1$  to  $2T$  so that we can exclude as many transient states as possible. This enables us to get more stable values of  $p_0^{(i)}$  ( $p_1^{(i)}$ ) by focusing on states closer to or belonging to attractors (Figure S1 in Supplementary Material). Figure 3 shows an example of computing  $E$  in a Boolean network.

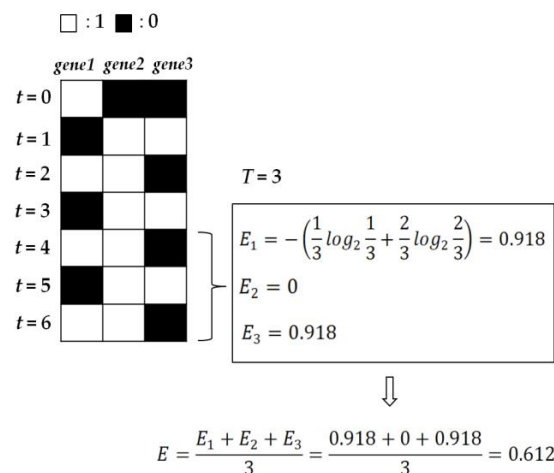


**Figure 3.** An example showing how to calculate the emergence of each node and the average,  $E$ . Since average emergence  $E$  (of the network) is 0.612, the complexity  $C$  is  $4 \times 0.612 \times (1 - 0.612) \cong 0.95$ . With initial configuration 100, the state transitions were obtained from  $t = 0$  to  $t = 6$  in the example RBN of Figure 1.

In Equation (2),  $C$  has the maximum value of 1 when  $E$  is 0.5 [68,69]. For example, under the condition that all the nodes of a Boolean network have the same emergence values, when  $p_0$  or  $p_1$  is around 0.89, average  $E$  becomes 0.5. In contrast,  $C$  has the minimum value of 0 for a node when  $E$  is 1 (constant change) or 0 (no change). Under the condition that all the nodes have the same emergence values, when  $p_0$  and  $p_1$  are 0.5 or when  $p_0$  or  $p_1$  is 1, average  $E$  of a network becomes 1 or 0, respectively.

As seen in the examples, complexity is determined by how 1 and 0 s are distributed during state transitions. The distribution of 1 and 0 s at each node represents how node states are altered and kept. Thus, the complexity of Boolean networks measures a degree of the balance ( $E = 0.5$ ) between change ( $E = 1$ ) and regularity ( $E = 0$ ) of gene expression information.

### 2.3.2. External Perturbations to Boolean Networks

We consider flipping the node states of the networks as external perturbations so as to measure antifragility [23,24] (as opposed to the internal perturbations, i.e., mutations, described above). The degree of external perturbations ( $\Delta x$ ) is quantified by the following equation:

$$\Delta x = \frac{X \times \left(\frac{T}{O}\right)}{N \times T} = \frac{X}{N \times O} \quad (4)$$

where  $X$  is the number of nodes randomly chosen to be perturbed,  $T$  is the simulation time for state transitions, and  $O$  is the perturbation frequency which determines how many time steps are executed between perturbations.  $X$  nodes are randomly chosen and perturbed every time step of  $O$ . For instance, if  $N = 10$ ,  $X = 4$ ,  $T = 5$ , and  $O = 1$ , we randomly choose four nodes ( $X = 4$ ) in a network with 10 nodes ( $N = 10$ ) and then change the states of the selected nodes. We repeat this perturbation every time step ( $O = 1$ ) during  $2 \times 5 = 10$  time steps ( $T = 5$ ). Here, perturbing the network during not five but 10 time steps is because we are interested in state transitions from  $T + 1$  to  $2T$  as mentioned in Section 2.3.1.

$\Delta x$  has the interval  $[0,1]$  ( $0 \leq \Delta x \leq 1$ ). This term is used to adjust the influence of network size on antifragility. In the simulations, the parameters are set to  $X = [1, 2, \dots, N]$ ,  $T = 200$ , and  $O = 1$ . The values of  $T$  and  $O$  were determined based on our previous research [23]: If  $T$  is large enough, the shape of the antifragility curve is consistently obtained over  $T$  (with  $T$  increasing). In other words, antifragility curves quickly converge with an increasing  $T$ . For Boolean networks which have less than 100 nodes,  $T = 200$  was enough to measure antifragility.  $O = 1$  showed the most distinctive difference of antifragility between networks. As with other variables related to our antifragility measure, the time required to perform these calculations increases linearly with  $N$ .

### 2.3.3. Antifragility of Boolean Networks

Our antifragility measure ( $\phi$ ) is composed of two terms: The difference of “satisfaction” before and after external perturbations ( $\Delta\sigma$ ) and the degree of external perturbations ( $\Delta x$ ) [23,24]. The equation is as follows:

$$\phi = -\Delta\sigma \times \Delta x, \quad (5)$$

Here, the degree of external perturbations ( $\Delta x$ ) was explained in Section 2.3.2. To obtain the difference of satisfaction before and after external perturbations ( $\Delta\sigma$ ), the concept of satisfaction ( $\sigma$ ) should be explained.  $\sigma$  represents how much the “goal” of agents has been attained [70]. The agents and goal can be defined differently depending on systems and observers. In Boolean networks, each node can be regarded as an agent. Their goal can be arbitrarily defined as achieving high complexity.

For Equation (5),  $\Delta\sigma$  is calculated by the following equation:

$$\Delta\sigma = C - C_0, \quad (6)$$

where  $C_0$  and  $C$  are the complexities before and after external perturbations, respectively.  $\Delta\sigma$  has values in the range  $[-1, 1]$  ( $-1 \leq \Delta\sigma \leq 1$ ) as  $C_0$  and  $C$  have the interval  $[0,1]$ . Thus, if  $\Delta\sigma$  is positive ( $C \geq C_0$ ), it means that complexity was increased by the external perturbations. That is, we define “benefiting from perturbations” as increasing their complexity. If this is the case, the Boolean network can be considered antifragile. If  $\Delta\sigma$  is negative ( $C \leq C_0$ ), it indicates that complexity decreases by external perturbations. It can be seen as fragile. If  $\Delta\sigma$  is zero ( $C = C_0$ ), complexity is maintained against external perturbations. Thus, the network can be regarded as robust.

To calculate  $C_0$  and  $C$ , when the state transitions of the original network and perturbed one are computed, the same initial states are used at  $t = 0$ . Depending on the initial states, because complexity can be different,  $C_0$  and  $C$  are calculated as the average of the complexity values acquired from a large number of initial conditions that are randomly chosen. This yields a more stable value of  $\phi$  as a system property. In our simulations, the number of initial states ( $s$ ) is set to 1000.

#### 2.4. Property Classification with a Convolutional Neural Network

We tried several classification methods, including multinomial logistic regression (46.33% accuracy), and a convolutional neural network (CCN) was the most effective.

##### 2.4.1. Input and Output in a CNN

We use a CNN to classify the properties of the biological networks into the four classes: Not robust & not evolvable, not robust & evolvable, robust & not evolvable, and robust & evolvable. In our CNN model, the input consists of the differences of antifragility between the original and mutated networks, and the output consists of the properties classified into the four classes. As we use 37 biological networks and add the internal perturbations 1000 times to each network, we have  $37 \times 1000 = 37,000$  quantities of the differences of antifragility and the classified properties, respectively.

We explain how to obtain the input, taking the Mammalian cell cycle network with 20 nodes and its mutated network as examples. Figure 4a,b show the antifragility of the two networks depending on the number of perturbed nodes  $X$ . We interpolate to get 30 data points for each network (independently of  $N$ ) and subtract the antifragility value of the mutated network from that of the original network at each data point. Then, we get 30 difference values in the normalized range  $[1/N, 1 (=N/N)]$  (Figure 4c). In this way, for all the networks with the different number of nodes, we can get 37,000 input elements in which one element is composed of 30 data points. This process allows antifragility of all the networks to have the same size of  $30 \times 1$ . This shape of input is necessary to use CNNs which require images with the same width and height as input.

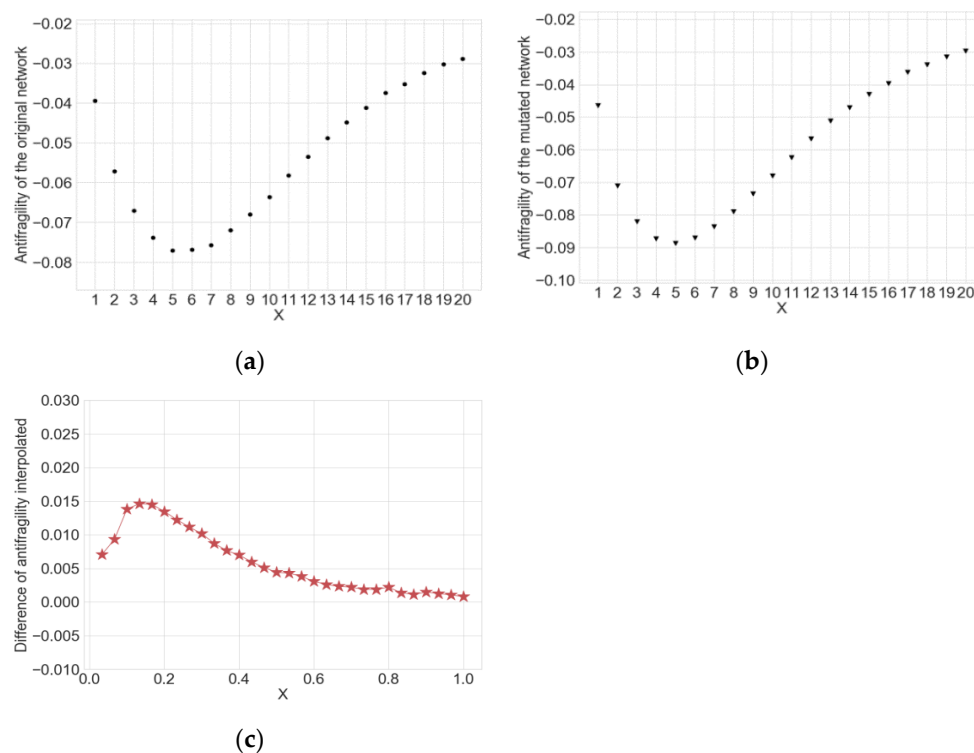


**Figure 4.** Data points related to antifragility of the mammalian cell cycle network with  $N = 20$ . In the simulations, the parameters were set to perturbed node size  $X = [1, 2, \dots, 20]$ , simulation time for state

transitions  $T = 200$ , perturbation frequency  $O = 1$ : (a) 20 data points on antifragility of the original network; (b) 20 data points on antifragility of the mutated network; (c) 30 data points on the differences of antifragility estimated through interpolation in the normalized range.

### 2.4.2. Nested $k$ -Fold Cross-Validation

We carry out nested  $k$ -fold cross validation to select a model and evaluate the model performance. Figure 5 briefly illustrates the process of the cross-validation. We split the data with the 37,000 quantities into training data (i.e.,  $37,000 \times 0.75 = 27,750$ ) and test data (i.e.,  $37,000 \times 0.25 = 9250$ ) with the ratio of 75 to 25 and set  $k = 4$  (Outer loop A in Figure 5). However, the data about the properties labeled with the four classes is imbalanced, as the four classes are not equally distributed. Thus, we have a multiclass classification problem with imbalanced data. We balance the training data using an oversampling technique. We get balanced data that make up the same number of samples per class. Then, we divide the balanced data into training data and validation data with the ratio of 67 to 33 (Inner loop in Figure 5). From  $k = 1$  to  $k = 4$ , we train our model with the balanced data and test it with the original imbalanced data for each fold (Outer loop B in Figure 5).

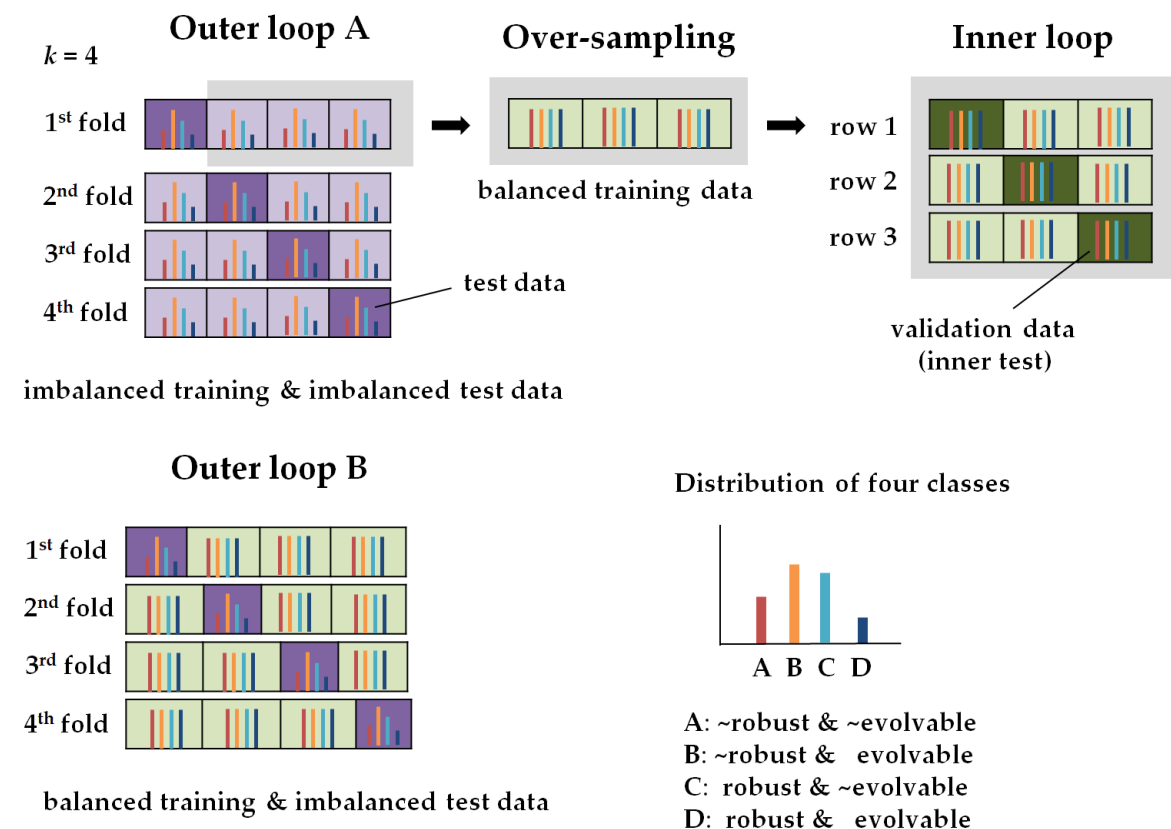


**Figure 5.** The illustration for the processes of the nested  $k$ -fold cross-validation ( $k = 4$ ). In the inner loop, the values of the hyperparameters are set and the model parameters are fitted. In the outer loop, the model performance is evaluated.

We have three hyperparameters: Batch size = {32, 64, 128}, data balancing = {SMOTE, ADASYN}, and CNN architecture = {simple, complex}. For the data balancing, we try SMOTE (Synthetic Minority Over-Sampling Technique) and ADASYN (Adaptive Synthetic Sampling Approach), which are oversampling techniques generating synthetic samples from the minority class [71,72]. Regarding the architecture, we try a simple CNN model and a complex one. CNN is usually composed of the convolutional layer (Conv) with a rectified linear unit (ReLU) activation function, pooling layer (Pool), flattening layer (Flat), fully connected layer (FC), and output layer (Out). The layers are arranged in

the order of Conv + ReLU-Pool-Flat-FC-Out. Depending on how many Conv + ReLU-Pool layers are stacked, CNNs become deeper neural networks. The deeper CNNs can handle higher resolution images. In our study, the simple CNN has Conv-Conv + ReLU-Pool, and the complex CNN has Conv + ReLU-Conv + ReLU-Pool-Conv + ReLU-Conv + ReLU-Pool (Figure 6).

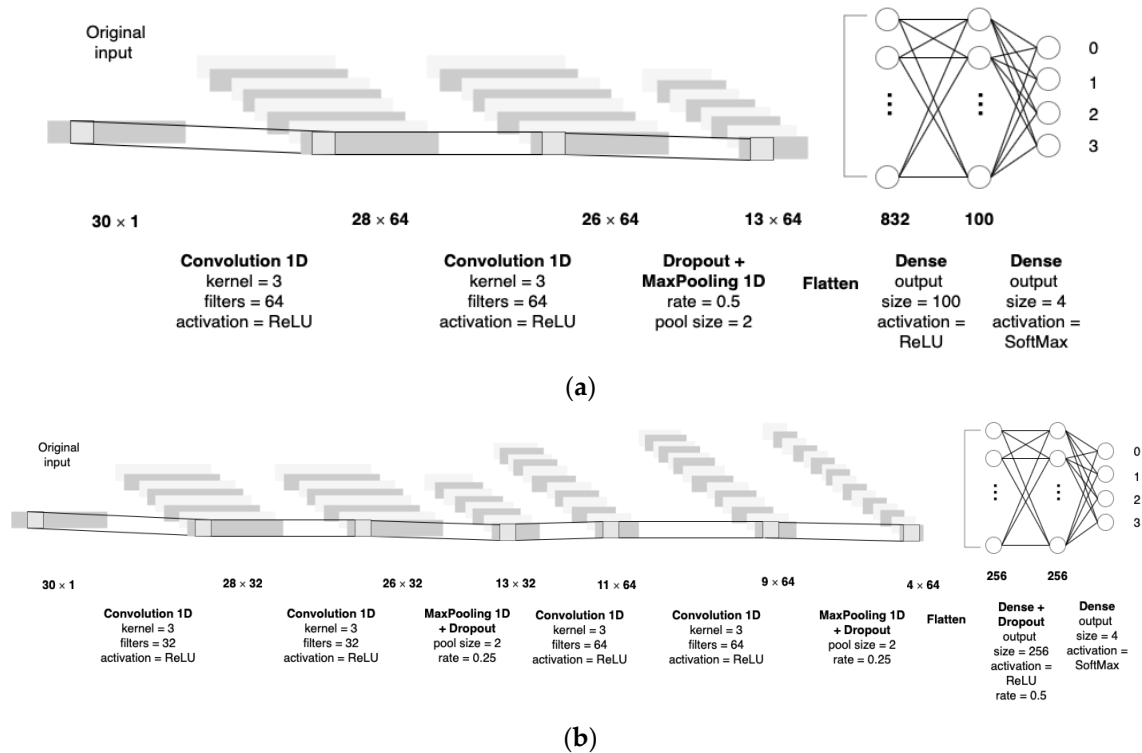


**Figure 6.** Convolutional neural network (CNN) architectures for simulations. (a) Our simple CNN model has two convolution layers, and one pooling layer. (b) Our complex CNN model has four convolution layers and two pooling layers.

- Inner loop: We set the values of hyperparameters and fit the model parameters. The model is trained and validated with the balanced data. We use AUC (i.e., area under the ROC curve) as a criterion to find the best hyperparameter set. We have 12 hyperparameter sets in total (Table 2 and Figure 6). For the three rows of the inner loop derived from the first fold in Figure 5, we calculate  $AUC = \{AUC(\text{hyp1}), AUC(\text{hyp2}), \dots, AUC(\text{hyp12})\}$  in the validation of each row, and then get averages over the three rows (i.e.,  $AUC^{\text{avg}} = \{AUC(\text{hyp1})^{\text{avg}}, AUC(\text{hyp2})^{\text{avg}}, \dots, AUC(\text{hyp12})^{\text{avg}}\}$ ). Repeating the process from the second fold to the fourth one, we get their means for the four folds (i.e.,  $AUC^{\text{final}} = \{AUC(\text{hyp1})^{\text{final}}, AUC(\text{hyp2})^{\text{final}}, \dots, AUC(\text{hyp12})^{\text{final}}\}$ ). Finally, we selected hyp 2 as the best hyperparameter set from the values of  $AUC^{\text{final}}$  in Table 2.
- Outer loop: We train the model which has the optimal parameters determined from the inner loop. The model is trained with the balanced data. Tables 3 and 4 show the accuracy of the training and validation dataset, respectively. After training the model, we test it with the original imbalanced data (Outer loop B in Figure 5). To evaluate the model performance, we get a test accuracy, a confusion matrix, and precision-recall (PR) curves. They are averages over the four folds.

**Table 2.** Twelve hyperparameter sets for the simulations in the inner loop.

Set	Epoch	Batch Size	Balancing	Architecture	AUC <sup>final</sup>
hyp1	128	32	SMOTE	simple	0.8265
hyp2	128	64	SMOTE	simple	0.8295
hyp3	128	128	SMOTE	simple	0.8251
hyp4	128	32	SMOTE	complex	0.8075
hyp5	128	64	SMOTE	complex	0.8101
hyp6	128	128	SMOTE	complex	0.8056
hyp7	128	32	ADASYN	simple	0.8151
hyp8	128	64	ADASYN	simple	0.8124
hyp9	128	128	ADASYN	simple	0.8137
hyp10	128	32	ADASYN	complex	0.7922
hyp11	128	64	ADASYN	complex	0.7931
hyp12	128	128	ADASYN	complex	0.7941

**Table 3.** Training accuracy.

	Row 1	Row 2	Row 3
<b>1st fold</b>	0.7266	0.7288	0.6929
<b>2nd fold</b>	0.7410	0.7362	0.7433
<b>3rd fold</b>	0.7324	0.7085	0.7134
<b>4th fold</b>	0.6889	0.7030	0.7212
	avg. = 0.7197		

**Table 4.** Validation accuracy.

	Row 1	Row 2	Row 3
<b>1st fold</b>	0.5688	0.5802	0.5815
<b>2nd fold</b>	0.5965	0.5661	0.6003
<b>3rd fold</b>	0.6078	0.5828	0.5547
<b>4th fold</b>	0.5682	0.5742	0.5630
	avg. = 0.5787		

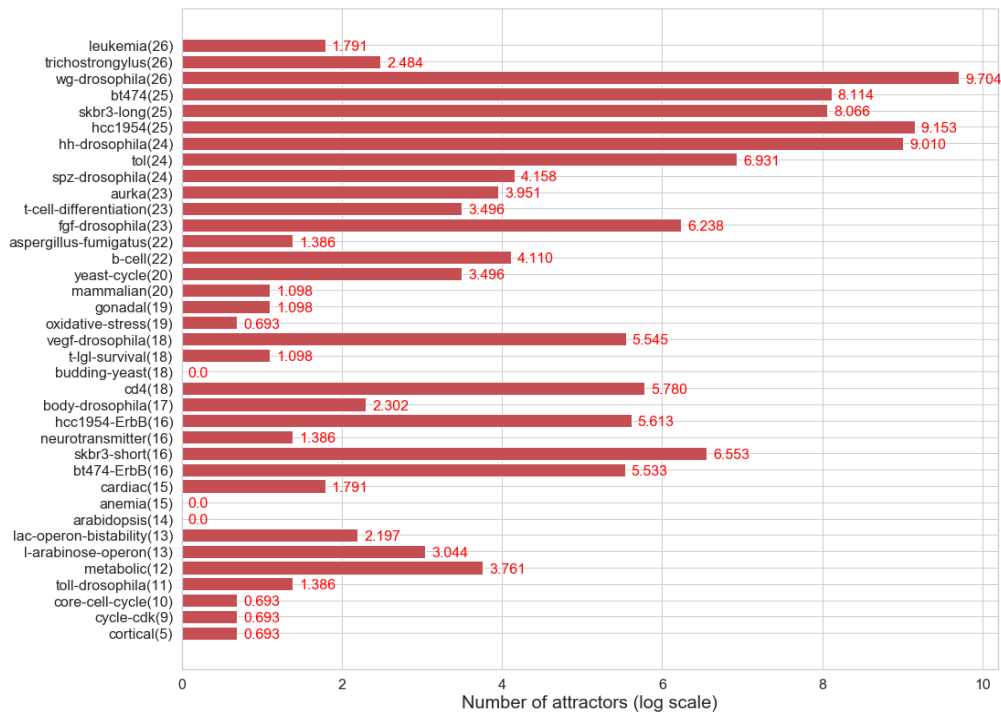
### 3. Results

#### 3.1. Attractors and Basins of Attraction of Biological Networks

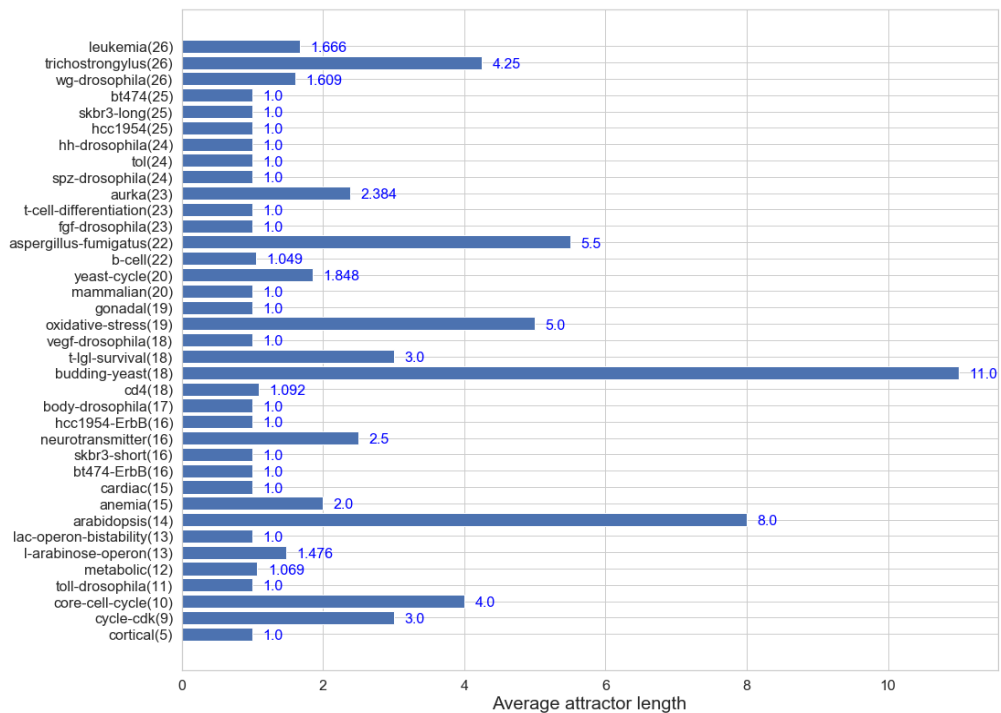
We explored the attractors and basins of attraction to find the structural features of the state space in the Boolean network models of the 37 biological systems. Specifically, we measured the number of attractors, the average length of attractors, and the normalized basin entropy. In the case of the normalized basin entropy, it was calculated by dividing Krawitz et al.'s measure [73] by the number of nodes (i.e.,  $H = -\sum_{\rho} p_{\rho} \log_2 p_{\rho} / N$  where  $p_{\rho}$  is the basin size of attractor  $\rho$  divided by state space size  $2^N$ ,  $\sum_{\rho} p_{\rho} = 1$ ). This is normalized between 0 and 1. As mentioned in the introduction, the attractors can represent cell types or functions [15–17]. Hence, from a biological viewpoint, the number of attractors can be interpreted as the number of cell functions, and the average length of attractors can be regarded as the time that it takes cell functions to be conducted. The normalized basin entropy can be seen as the versatility of cell functions because it provides information about the distribution of basin sizes. The more even the basin sizes of attractors are in the state space, the larger the value of normalized entropy is. In the case that all basins of attraction have similar size, when initial states are changed by noise, they are more likely to converge different attractors by jumping from one basin to another.

Figure 7a shows the distribution of the number of attractors in log scale. It is clear that various biological systems have different numbers of cell functions. Figure 7b displays the distribution of the average length of attractors. Overall, more than half of the networks have only fixed-point attractors, and the rest of them have relatively short cyclic attractors when their state space sizes are considered.

The values varied between 1 and 11, indicating that each biological system spends different times carrying out its cellular function(s). Figure 7c presents the distribution of the normalized basin entropy. The values are diversely distributed between 0 and 0.541. This indicates that some biological systems perform only a few cell functions dominantly, while others commonly change the cell functions among many ones.



(a)



(b)

Figure 7. Cont.

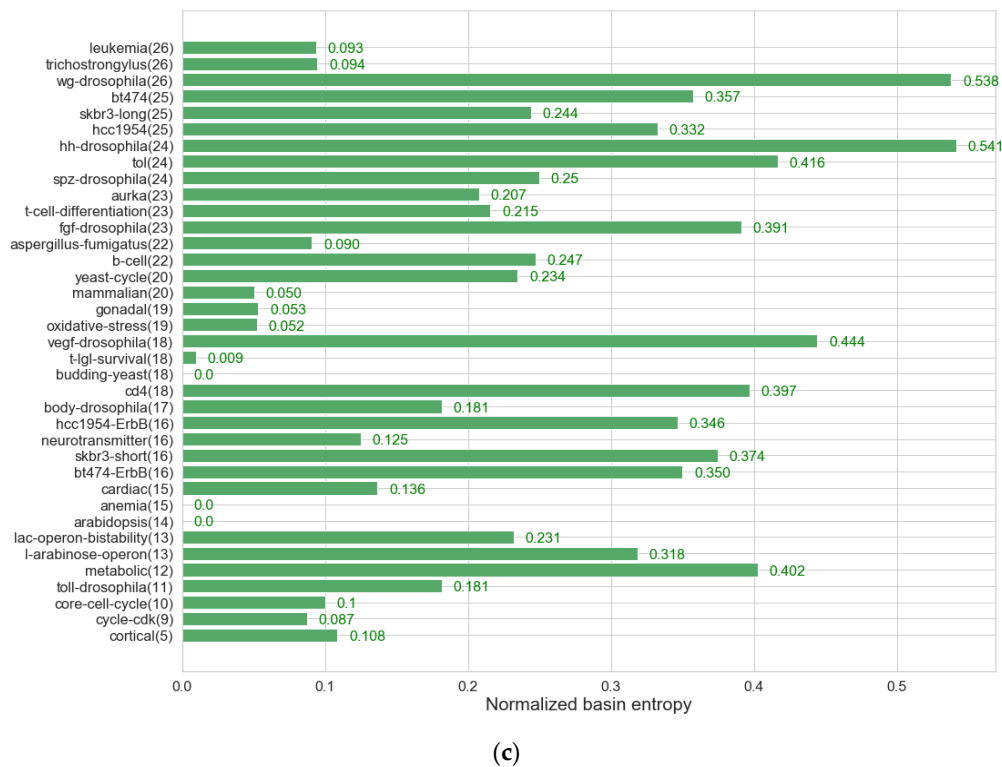


**Figure 7.** Attractors and basins of attraction of the 37 biological networks. The number in the parenthesis on the  $y$ -axis points out the number of nodes of the network: (a) The number of attractors. The values took the natural logarithm ( $e \cong 2.718$ ) so 0 means that the biological network has a single attractor; (b) the average length of attractors; (c) normalized basin entropy. It has the range [0, 1]. The more even the basin sizes of attractors are in the state space, the larger the value normalized entropy will have.

All three measures have large value variations, so it is difficult to find common structural features of the state space. These biological systems are specialized for their different cell functions, which may cause such variations. From the variations, we can see that there exists biological networks that have a broad variety of number of attractors, attractor lengths, and basin distributions. For these networks, it is computationally difficult to study the robustness and evolvability of biological systems by comparing the attractors before and after perturbations. It is even harder for larger biological networks because the number of attractors, the attractor length, and the basin size will increase as the number of nodes grows. Therefore, it is necessary to estimate the robustness and evolvability of biological networks without measuring attractors exhaustively.

### 3.2. Distribution of the Four Classes on Robustness and Evolvability of Biological Networks

We classified the robustness and evolvability of the 37 biological networks into the four classes (not robust & not evolvable, not robust & evolvable, robust & not evolvable, robust & evolvable) to investigate how the biological networks respond to mutations. Figure 8 shows the percentage frequency distribution of the four classes. For each biological network, we added a different internal perturbation 1000 times, and thus acquired the percentage frequency from 1000 different mutated networks.

As seen in Figure 8, every biological network has three, or four classes. Overall, the class of robust & evolvable takes up the lowest percentage. The classes of not robust & evolvable and robust & not evolvable account for the majority of the percentage. The only class that is not present in all networks is not robust & not evolvable. These findings propose that a biological system can display different behaviors of robustness and evolvability against mutations. Furthermore, it is known that biological systems are robust and evolvable [1–6], which could be explained not from the behavior of robust & evolvable but the two dynamical behaviors of not robust & evolvable and robust & not evolvable.

In other words, it is highly likely that mutations will lead to robust or evolvable networks. It can also be argued that a more complex mechanism is required for being at the same time robust & evolvable, so this could explain why not many networks exhibit both properties frequently.

In addition, such distribution of the dynamical responses suggests evolutionary profiles of what the environments given to the biological systems were like. Not robust & evolvable makes up the highest percentage frequency of the four classes in the distribution, which implies that many biological systems might have been mainly exposed to drastic environmental changes hard to keep the existing cell functions, and thus evolved towards preferring producing brand new cell functions to adapt to the new environments.

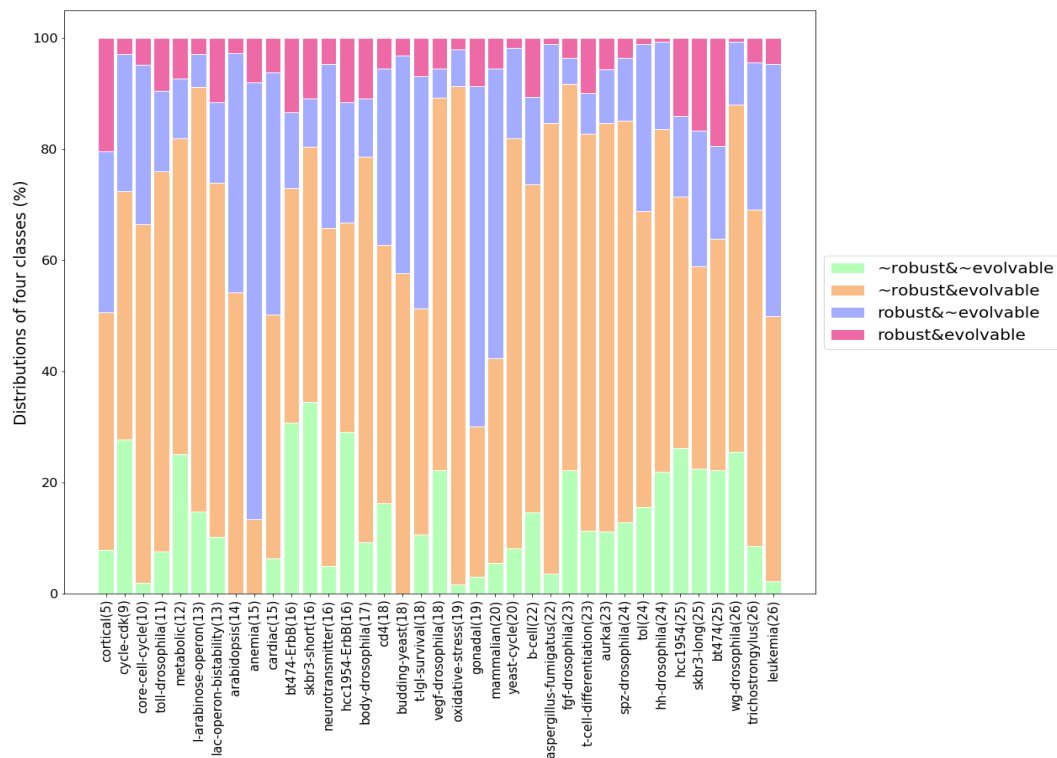


**Figure 8.** Percentage frequency distribution of the four classes on robustness and evolvability for the 37 biological networks. A different internal perturbation was added to each network 1000 times, so 1000 different mutated networks were generated per biological network. The perturbed networks were classified into not robust & not evolvable, not robust & evolvable, robust & not evolvable, or robust & evolvable.

### 3.3. Association between Mutation Type and Robustness and Evolvability

We computed Cramer's  $V$  to measure the strength of association between the mutation type and the robustness and evolvability. We had the four mutation types: Adding a link (add), deleting a link (delete), changing the position of a link (change), and flipping one state in a Boolean function (flip). We randomly chose one mutation type and then added it to the biological network. This process was repeated 1000 times per biological network, so we obtained 37,000 pairs (mutation type, property class) for the 37 biological networks. Table 5 is a contingency table displaying the frequency distribution of the four classes depending on the mutation type. From the table, we got Cramer's  $V = 0.2292$ . Cramer's  $V$  takes values from 0 to 1. The closer to zero, the weaker the association between the variables. Hence, we found that there is a weak association between the mutation type and the property class. This indicates that the type of genetic mutations do not have a strong effect on determining the robustness and evolvability of biological systems.

**Table 5.** A contingency table for the four classes depending on the mutation type.

	Add	Delete	Change	Flip
<b>not robust &amp; not evolvable</b>	2180	549	1731	532
<b>not robust &amp; evolvable</b>	11443	1204	6067	1889
<b>robust &amp; not evolvable</b>	2380	642	1873	3893
<b>robust &amp; evolvable</b>	958	241	754	664

### 3.4. Prediction of Robustness and Evolvability Using Antifragility

We got a test accuracy, confusion matrix, and precision-recall curves for the test data to evaluate the performance of our CNN model. We preferred using precision-recall (PR) curves to receiver operating characteristic (ROC) curves because we tested the model with the imbalanced data [74].

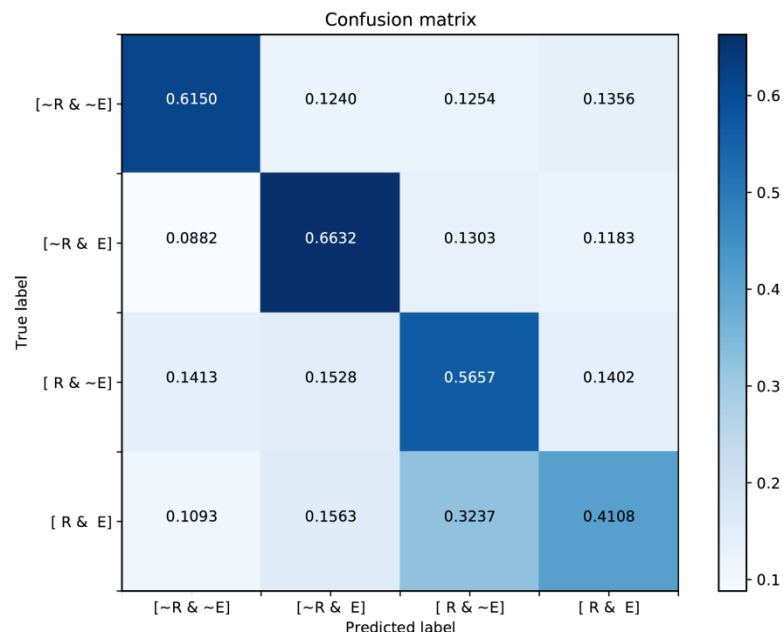
Table 6 presents a test accuracy. The overall accuracy is 0.5845. Figure 9a shows a normalized confusion matrix. In the confusion matrix, the  $x$ -axis refers to an instance of the predicted classes, and the  $y$ -axis represents an instance of the actual classes. The values of the diagonal elements mean the probability of correctly predicted classes. For each class, not robust & not evolvable is 0.6150, not robust & evolvable is 0.6632, robust & not evolvable is 0.5657, and robust & evolvable is 0.4108. From the accuracy and confusion matrix, we can see that our model has a satisfactory performance for the classification of robustness and evolvability.

Figure 9b exhibits a micro-averaged PR curve for the four classes. We computed the micro-average globally not distinguishing the elements between different classes, which is usually preferable for imbalanced classes. In our PR curve, the average precision (AP) is 0.54. This score refers to the area under the PR curve. To compute AP, the function of `average_precision_score` was used in the scikit-learn library of Python ([https://scikit-learn.org/stable/auto\\_examples/model\\_selection/plot\\_precision\\_recall.html#sphx-glr-auto-examples-model-selection-plot-precision-recall-py](https://scikit-learn.org/stable/auto_examples/model_selection/plot_precision_recall.html#sphx-glr-auto-examples-model-selection-plot-precision-recall-py)). The large AP means high precision and high recall. High precision is related to a low false positive rate (type I error  $\alpha$ ) and high recall is related to a low false negative rate (type II error  $\beta$ ).

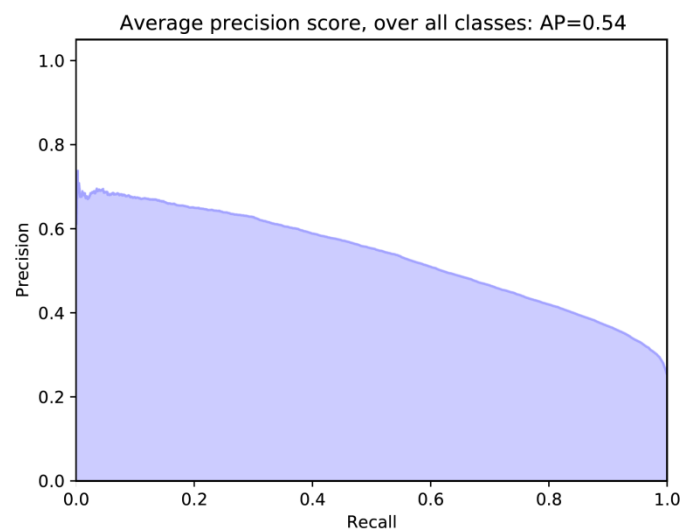
Overall, our model has a good performance but there are differences for each class. Figure 10 shows PR curves per class. Not robust & not evolvable has AP = 0.52 (Figure 10a), not robust & evolvable has AP = 0.64 (Figure 10b), robust & not evolvable has AP = 0.81 (Figure 10c), and robust & evolvable has AP = 0.17 (Figure 10d). The three classes of not robust & not evolvable, not robust & evolvable, and robust & not evolvable have larger AP values when compared to the class of robust & evolvable. It indicates that our classifier not only detects a majority of the positive results for the three classes but also classifies them correctly. Meanwhile, robust & evolvable has the smallest AP value. It might be a result of the scarcity of data on robust & evolvable, as seen in Figure 8, and/or a high variance of the differences of antifragility classified into robust & evolvable. These two things might have made it hard for our CNN model to find the feature map of robust & evolvable.

**Table 6.** Test accuracy.

<b>1st fold</b>	0.5794
<b>2nd fold</b>	0.5676
<b>3rd fold</b>	0.5897
<b>4th fold</b>	0.6015
	avg. = 0.5845



(a)



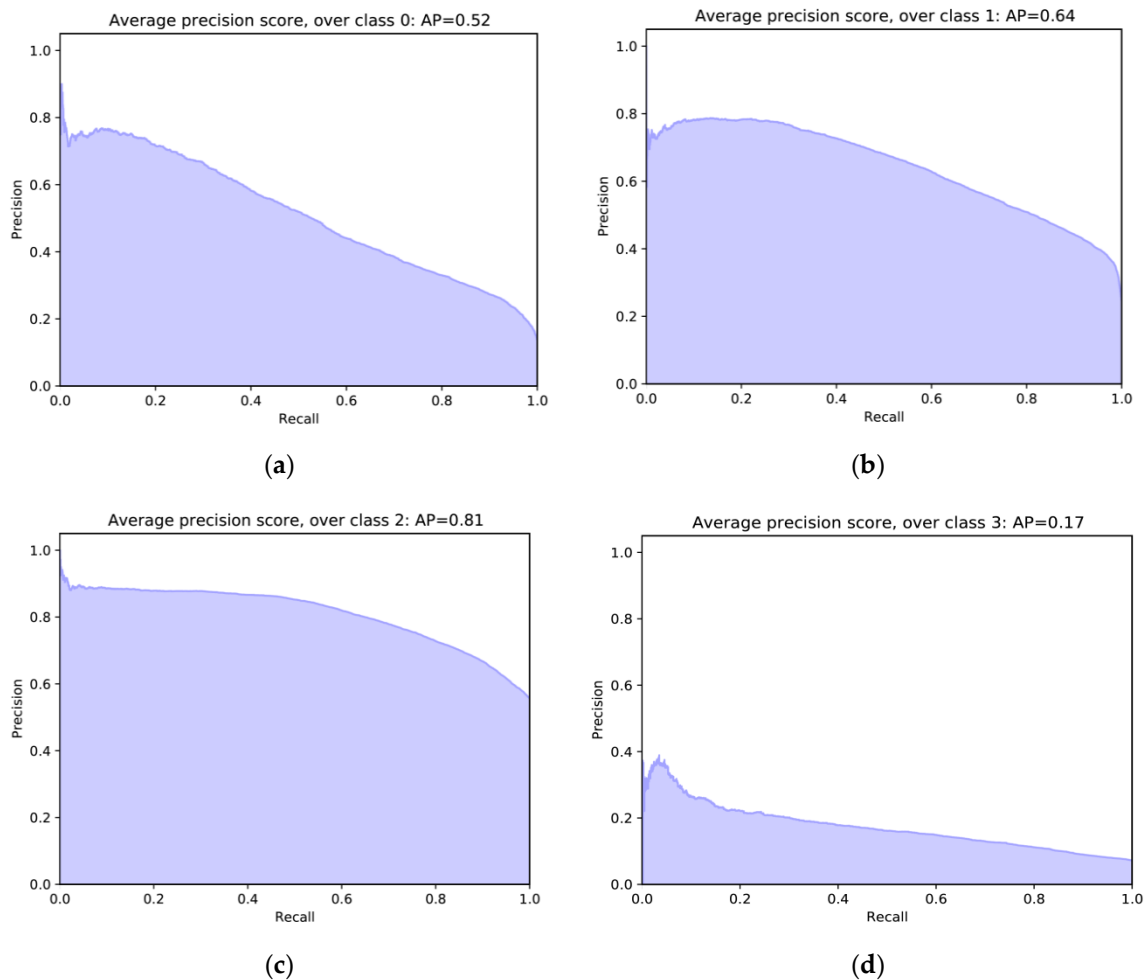
(b)

**Figure 9.** Model evaluation: (a) Normalized confusion matrix; (b) micro-averaged precision-recall curve for the four classes and its average precision (AP) score for the test data.

Table 7 shows the AP values between our model and random classifiers. In PR curves, the AP of random classifiers is 0.5 only when there are two classes and their distributions are balanced. For binary classification of balanced and imbalanced datasets, the AP of random classifiers is defined as positive/(positive + negative) [63,74]. Our test data is imbalanced, so we computed the AP values of random classifiers based on the ratio of positive and negative. Since output is binarized when the PR curve and AP are extended to multi-class classification, calculating the AP values of our model and random classifiers is regarded as binary classification for each class. Table 7 demonstrates that all the AP values for the four classes in our model are larger than those of random classifiers. Although the class of robust & evolvable has a relatively smaller AP value than the other classes, our model has better performance to classify all the classes than random classifiers.

**Table 7.** Comparison of AP values between our model and random classifiers.

	AP of Our Classifier	AP of Random Classifier
<b>not robust &amp; not evolvable</b>	0.52	0.135
<b>not robust &amp; evolvable</b>	0.64	0.557
<b>robust &amp; not evolvable</b>	0.81	0.238
<b>robust &amp; evolvable</b>	0.17	0.071

**Figure 10.** Precision-recall curves and average precision (AP) scores for the four classes for the test data: (a) Not robust & not evolvable; (b) not robust & evolvable; (c) robust & not evolvable; (d) robust & evolvable.

#### 4. Discussion

In this study, we classified robustness and evolvability in Boolean network models of biological systems into the four classes: Not robust & not evolvable, not robust & evolvable, robust & not evolvable, and robust & evolvable. The classification was defined based on the change of attractors representing cell fates or cell functions before and after mutations. Using antifragility which is simply calculated from the dynamics during state transitions following external perturbations, we proposed a classifier to predict the properties of the four classes. We used a convolutional neural network, where the input is the difference of antifragility between original networks and their mutated ones and the output is the four classes. Our model showed a good performance for the multi-class classification. It indicates that our antifragility measure can play a role of a predictor to estimate the robustness and evolvability of biological networks.

To evaluate the utility of our antifragility in terms of a computational cost, we measured the computation time of finding attractors and calculating antifragility. When searching for all attractors, we used Dubrova and Teslenko's algorithm which is a SAT-based approach to find attractors efficiently in synchronous Boolean networks [75]. This algorithm has two steps to find attractors. In the first step, a problem is encoded as input for the SAT solver. In the second step, the problem is solved by the SAT solver. However, SAT is NP-complete so the NP-complete problem is intractable in the worst case scenario due to exponential complexity in the encoding or solving phase. For the 37 biological networks with less than 30 nodes in our study, finding attractors was faster than calculating antifragility (Figure S3 in Supplementary Material). However, we tried to compute the attractors and antifragility of lymphocytic leukemia with 91 nodes ( $2^{91}$  possible states) collected from Cell Collective. While it took about 47 min to calculate its antifragility value, we could not get its attractors even after a few days in our cluster equipped with 132 G memory. Similar to lymphocytic leukemia, in some large Boolean networks, finding all attractors is computationally expensive or even unfeasible because of very long attractor lengths or a large number of attractors as the state space size is exponentially increased by the growing number of nodes. As the state space size is  $2^N$ , memory simply runs out if one attempts to explore exhaustively large networks. In this case, our classifier with antifragility can be a useful tool for studying the robustness and evolvability of biological networks, as it requires only a sample of the dynamics of original and perturbed networks.

For further study, we plan to use more data. We will collect more kinds of biological Boolean networks, introduce artificial data generated from random Boolean networks and add more mutations to the networks. Since the amount of data is one of important factors to have an influence on model performance, we will run simulations with more extensive data to find the better classifier. In addition, we will thoroughly explore the relationship between antifragility and robustness/evolvability. One possibility is that because antifragility reflects the characteristics of basins of attraction (e.g., the structure of basins of attraction) and attractors (e.g., the number and length of attractors), it might work for predicting the preservation and emergence of attractors. However, to reveal the relationship more clearly, we need further explorations. Taking a step forward, we will evolve random networks using antifragility as a fitness function and examine the robustness and evolvability of the resulting networks. This future research could give a clue to the mechanism of how biological systems obtained robustness and evolvability, and also suggest a possibility for developing robust and/or evolvable engineered systems which have antifragility as a control parameter.

**Supplementary Materials:** The following are available online at <http://www.mdpi.com/1099-4300/22/9/986/s1>, Figure S1: Histograms of transient lengths: how many state transitions all state configurations go through until they reach attractors. For the 37 biological networks, the maximum is 31 in aurka, which means that every state configuration of all biological networks converges to attractors within 32 state transitions. This implies that the basins of attraction of biological networks tend to be relatively shallow, Figure S2: Time complexity of calculating antifragility. It linearly increases with the number of nodes (N), Figure S3: Comparison of computation time between calculating antifragility and finding attractors for the 37 biological networks.

**Author Contributions:** Conceptualization, H.K. and C.G.; methodology, H.K. and S.M.; software, H.K., S.M., and P.O.; formal analysis, H.K., S.M., and P.O.; data curation, H.K. and S.M.; writing—original draft preparation, H.K.; writing—review and editing, H.K., S.M., P.O., and C.G.; visualization, H.K., S.M., and P.O.; supervision, C.G.; project administration, C.G.; funding acquisition, C.G. All authors have read and agreed to the published version of the manuscript.

**Funding:** This work was partially supported by UNAM's PAPIIT projects IN107919 and IV100120.

**Conflicts of Interest:** The authors declare no conflict of interest. The funders had no role in the design of the study; in the collection, analyses, or interpretation of data; in the writing of the manuscript, or in the decision to publish the results.

## References

- De Visser, J.A.G.; Hermisson, J.; Wagner, G.P.; Meyers, L.A.; Bagheri-Chaichian, H.; Blanchard, J.L.; Chao, L.; Cheverud, J.M.; Elena, S.F.; Fontana, W. Perspective: Evolution and detection of genetic robustness. *Evolution* **2003**, *57*, 1959–1972. [[CrossRef](#)]
- Kirschner, M.; Gerhart, J. Evolvability. *Proc. Natl. Acad. Sci. USA* **1998**, *95*, 8420–8427. [[CrossRef](#)]
- Nehaniv, C.L. Evolvability. *BioSystems* **2003**, *2*, 77–81. [[CrossRef](#)]
- Poole, A.M.; Phillips, M.J.; Penny, D. Prokaryote and eukaryote evolvability. *Biosystems* **2003**, *69*, 163–185. [[CrossRef](#)]
- Stelling, J.; Sauer, U.; Szallasi, Z.; Doyle, F.J., III; Doyle, J. Robustness of cellular functions. *Cell* **2004**, *118*, 675–685. [[CrossRef](#)]
- Wagner, A. *Robustness and Evolvability in Living Systems*, 1st ed.; Princeton University Press: Princeton, NJ, USA, 2007; Volume 24.
- Wagner, A. Robustness and evolvability: A paradox resolved. *Proc. R. Soc. B Biol. Sci.* **2007**, *275*, 91–100. [[CrossRef](#)]
- Masel, J.; Trotter, M.V. Robustness and evolvability. *Trends Genet.* **2010**, *26*, 406–414. [[CrossRef](#)]
- Partha, R.; Raman, K. Revisiting robustness and evolvability: Evolution in weighted genotype spaces. *PLoS ONE* **2014**, *9*, e112792. [[CrossRef](#)]
- Elena, S.F.; Sanjuán, R. The effect of genetic robustness on evolvability in digital organisms. *BMC Evol. Biol.* **2008**, *8*, 284. [[CrossRef](#)]
- Whitacre, J.M. Degeneracy: A link between evolvability, robustness and complexity in biological systems. *Theor. Biol. Med. Model.* **2010**, *7*, 6. [[CrossRef](#)]
- Kitano, H. Biological robustness. *Nat. Rev. Genet.* **2004**, *5*, 826. [[CrossRef](#)] [[PubMed](#)]
- Levine, M.; Tjian, R. Transcription regulation and animal diversity. *Nature* **2003**, *424*, 147. [[CrossRef](#)]
- Aldana, M.; Balleza, E.; Kauffman, S.; Resendiz, O. Robustness and evolvability in genetic regulatory networks. *J. Theor. Biol.* **2007**, *245*, 433–448. [[CrossRef](#)] [[PubMed](#)]
- Chang, H.H.; Hemberg, M.; Barahona, M.; Ingber, D.E.; Huang, S. Transcriptome-wide noise controls lineage choice in mammalian progenitor cells. *Nature* **2008**, *453*, 544. [[CrossRef](#)]
- Huang, S.; Eichler, G.; Bar-Yam, Y.; Ingber, D.E. Cell fates as high-dimensional attractor states of a complex gene regulatory network. *Phys. Rev. Lett.* **2005**, *94*, 128701. [[CrossRef](#)]
- Huang, S. Gene expression profiling, genetic networks, and cellular states: An integrating concept for tumorigenesis and drug discovery. *J. Mol. Med.* **1999**, *77*, 469–480. [[CrossRef](#)]
- Kim, H.; Sayama, H. How criticality of gene regulatory networks affects the resulting morphogenesis under genetic perturbations. *Artif. Life* **2018**, *24*, 85–105. [[CrossRef](#)]
- Kim, J.; Vandamme, D.; Kim, J.-R.; Munoz, A.G.; Kolch, W.; Cho, K.-H. Robustness and evolvability of the human signaling network. *PLoS Comput. Biol.* **2014**, *10*, e1003763. [[CrossRef](#)]
- Torres-Sosa, C.; Huang, S.; Aldana, M. Criticality is an emergent property of genetic networks that exhibit evolvability. *PLoS Comput. Biol.* **2012**, *8*, e1002669. [[CrossRef](#)]
- Kim, H.; Sayama, H. Robustness and Evolvability of Multilayer Gene Regulatory Networks. In Proceedings of the 2018 Conference on Artificial Life, Tokyo, Japan, 23–27 July 2018; MIT Press: Tokyo, Japan, 2018; pp. 546–547.
- Taleb, N.N. *Antifragile: Things that Gain from Disorder*, 1st ed.; Random House Incorporated: New York, NY, USA, 2012; Volume 3.
- Pineda, O.K.; Kim, H.; Gershenson, C. A Novel Antifragility Measure Based on Satisfaction and Its Application to Random and Biological Boolean Networks. *Complexity* **2019**, *2019*. [[CrossRef](#)]
- Kim, H.; Pineda, O.K.; Gershenson, C. A Multilayer Structure Facilitates the Production of Antifragile Systems in Boolean Network Models. *Complexity* **2019**, *2019*. [[CrossRef](#)]
- Kauffman, S.A. Metabolic stability and epigenesis in randomly constructed genetic nets. *J. Theor. Biol.* **1969**, *22*, 437–467. [[CrossRef](#)]
- Kauffman, S.A. *The Origins of Order: Self-Organization and Selection in Evolution*, 1st ed.; Oxford University Press: New York, NY, USA, 1993.
- Kauffman, S. *At Home in the Universe: The Search for the Laws of Self-Organization and Complexity*; Reprint; Oxford University Press: New York, NY, USA, 1996.

28. Kim, H.; Sayama, H. The role of criticality of gene regulatory networks in morphogenesis. *IEEE Trans. Cogn. Dev. Syst.* **2018**. [[CrossRef](#)]
29. Escobar, L.A.; Kim, H.; Gershenson, C. Effects of Antimodularity and Multiscale Influence in Random Boolean Networks. *Complexity* **2019**, *2019*. [[CrossRef](#)]
30. Poblanno-Balp, R.; Gershenson, C. Modular random Boolean networks. *Artif. Life* **2011**, *17*, 331–351. [[CrossRef](#)] [[PubMed](#)]
31. Gershenson, C. Updating Schemes in Random Boolean Networks: Do They Really Matter. In *Artificial Life IX Proceedings of the Ninth International Conference on the Simulation and Synthesis of Living Systems, Boston, MA, USA, 12–15 September 2004*; MIT Press: Tokyo, Japan, 2004; pp. 238–243.
32. Roli, A.; Manfroni, M.; Pinciroli, C.; Birattari, M. On the Design of Boolean Network Robots. In *Proceedings of the European Conference on the Applications of Evolutionary Computation, Torino, Italy, 27–29 April 2011*; Springer: Berlin, Germany, 2011; pp. 43–52.
33. Muñoz, S.; Carrillo, M.; Azpeitia, E.; Rosenblueth, D.A. Griffin: A Tool for Symbolic Inference of Synchronous Boolean Molecular Networks. *Front. Genet.* **2018**, *9*, 39. [[CrossRef](#)]
34. Azpeitia, E.; Muñoz, S.; González-Tokman, D.; Martínez-Sánchez, M.E.; Weinstein, N.; Naldi, A.; Álvarez-Buylla, E.R.; Rosenblueth, D.A.; Mendoza, L. The combination of the functionalities of feedback circuits is determinant for the attractors' number and size in pathway-like Boolean networks. *Sci. Rep.* **2017**, *7*, 42023. [[CrossRef](#)]
35. Akutsu, T.; Hayashida, M.; Tamura, T. Algorithms for inference, analysis and control of Boolean networks. In *Proceedings of the International Conference on Algebraic Biology, Castle of Hagenberg, Austria, 31 July–2 August 2008*; Springer: Berlin, Germany, 2008; pp. 1–15.
36. Giacomantonio, C.E.; Goodhill, G.J. A Boolean model of the gene regulatory network underlying Mammalian cortical area development. *PLoS Comput. Biol.* **2010**, *6*, e1000936. [[CrossRef](#)]
37. Orlando, D.A.; Lin, C.Y.; Bernard, A.; Wang, J.Y.; Socolar, J.E.; Iversen, E.S.; Hartemink, A.J.; Haase, S.B. Global control of cell-cycle transcription by coupled CDK and network oscillators. *Nature* **2008**, *453*, 944. [[CrossRef](#)]
38. Fauré, A.; Naldi, A.; Chaouiya, C.; Thieffry, D. Dynamical analysis of a generic Boolean model for the control of the mammalian cell cycle. *Bioinformatics* **2006**, *22*, e124–e131. [[CrossRef](#)]
39. Mbodj, A.; Junion, G.; Brun, C.; Furlong, E.E.; Thieffry, D. Logical modelling of Drosophila signalling pathways. *Mol. Biosyst.* **2013**, *9*, 2248–2258. [[CrossRef](#)] [[PubMed](#)]
40. Steinway, S.N.; Biggs, M.B.; Loughran, T.P., Jr.; Papin, J.A.; Albert, R. Inference of network dynamics and metabolic interactions in the gut microbiome. *PLoS Comput. Biol.* **2015**, *11*, e1004338. [[CrossRef](#)] [[PubMed](#)]
41. Jenkins, A.; Macauley, M. Bistability and Asynchrony in a Boolean Model of the L-arabinose Operon in Escherichia coli. *Bull. Math. Biol.* **2017**, *79*, 1778–1795. [[CrossRef](#)] [[PubMed](#)]
42. Veliz-Cuba, A.; Stigler, B. Boolean models can explain bistability in the lac operon. *J. Comput. Biol.* **2011**, *18*, 783–794. [[CrossRef](#)]
43. Ortiz-Gutiérrez, E.; García-Cruz, K.; Azpeitia, E.; Castillo, A.; de la Paz Sanchez, M.; Álvarez-Buylla, E.R. A dynamic gene regulatory network model that recovers the cyclic behavior of Arabidopsis thaliana cell cycle. *PLoS Comput. Biol.* **2015**, *11*, e1004486. [[CrossRef](#)]
44. Rodríguez, A.; Torres, L.; Juárez, U.; Sosa, D.; Azpeitia, E.; García-de Teresa, B.; Cortés, E.; Ortiz, R.; Salazar, A.M.; Ostrosky-Wegman, P. Fanconi anemia cells with unrepaired DNA damage activate components of the checkpoint recovery process. *Theor. Biol. Med. Model.* **2015**, *12*, 19. [[CrossRef](#)]
45. Herrmann, F.; Groß, A.; Zhou, D.; Kestler, H.A.; Kühl, M. A boolean model of the cardiac gene regulatory network determining first and second heart field identity. *PLoS ONE* **2012**, *7*, e46798. [[CrossRef](#)]
46. Von der Heyde, S.; Bender, C.; Henjes, F.; Sonntag, J.; Korf, U.; Beissbarth, T. Boolean ErbB network reconstructions and perturbation simulations reveal individual drug response in different breast cancer cell lines. *BMC Syst. Biol.* **2014**, *8*, 75. [[CrossRef](#)]
47. Gupta, S.; Bisht, S.S.; Kukreti, R.; Jain, S.; Brahmachari, S.K. Boolean network analysis of a neurotransmitter signaling pathway. *J. Theor. Biol.* **2007**, *244*, 463–469. [[CrossRef](#)]
48. Marques-Pita, M.; Rocha, L.M. Canalization and control in automata networks: Body segmentation in Drosophila melanogaster. *PLoS ONE* **2013**, *8*, e55946. [[CrossRef](#)]

49. Martínez-Sánchez, M.E.; Mendoza, L.; Villarreal, C.; Alvarez-Buylla, E.R. A minimal regulatory network of extrinsic and intrinsic factors recovers observed patterns of CD4+ T cell differentiation and plasticity. *PLoS Comput. Biol.* **2015**, *11*, e1004324. [[CrossRef](#)] [[PubMed](#)]
50. Irons, D. Logical analysis of the budding yeast cell cycle. *J. Theor. Biol.* **2009**, *257*, 543–559. [[CrossRef](#)]
51. Saadatpour, A.; Wang, R.-S.; Liao, A.; Liu, X.; Loughran, T.P.; Albert, I.; Albert, R. Dynamical and structural analysis of a T cell survival network identifies novel candidate therapeutic targets for large granular lymphocyte leukemia. *PLoS Comput. Biol.* **2011**, *7*, e1002267. [[CrossRef](#)] [[PubMed](#)]
52. Sridharan, S.; Layek, R.; Datta, A.; Venkatraj, J. Boolean modeling and fault diagnosis in oxidative stress response. *BMC Genom.* **2012**, *13*, S4. [[CrossRef](#)] [[PubMed](#)]
53. Ríos, O.; Frias, S.; Rodríguez, A.; Kofman, S.; Merchant, H.; Torres, L.; Mendoza, L. A Boolean network model of human gonadal sex determination. *Theor. Biol. Med. Model.* **2015**, *12*, 26. [[CrossRef](#)] [[PubMed](#)]
54. Sahin, Ö.; Fröhlich, H.; Löbke, C.; Korf, U.; Burmester, S.; Majety, M.; Mattern, J.; Schupp, I.; Chaouiya, C.; Thieffry, D. Modeling ERBB receptor-regulated G1/S transition to find novel targets for de novo trastuzumab resistance. *BMC Syst. Biol.* **2009**, *3*, 1. [[CrossRef](#)]
55. Todd, R.G.; Helikar, T. Ergodic sets as cell phenotype of budding yeast cell cycle. *PLoS ONE* **2012**, *7*, e45780. [[CrossRef](#)]
56. Méndez, A.; Mendoza, L. A network model to describe the terminal differentiation of B cells. *PLoS Comput. Biol.* **2016**, *12*, e1004696. [[CrossRef](#)]
57. Brandon, M.; Howard, B.; Lawrence, C.; Laubenbacher, R. Iron acquisition and oxidative stress response in *Aspergillus fumigatus*. *BMC Syst. Biol.* **2015**, *9*, 19. [[CrossRef](#)]
58. Mendoza, L.; Xenarios, I. A method for the generation of standardized qualitative dynamical systems of regulatory networks. *Theor. Biol. Med. Model.* **2006**, *3*, 13. [[CrossRef](#)]
59. Dahlhaus, M.; Burkovski, A.; Hertwig, F.; Mussel, C.; Volland, R.; Fischer, M.; Debatin, K.-M.; Kestler, H.A.; Beltinger, C. Boolean modeling identifies Greatwall/MASTL as an important regulator in the AURKA network of neuroblastoma. *Cancer Lett.* **2016**, *371*, 79–89. [[CrossRef](#)] [[PubMed](#)]
60. Silva-Rocha, R.; de Lorenzo, V. The TOL network of *Pseudomonas putida* mt-2 processes multiple environmental inputs into a narrow response space. *Environ. Microbiol.* **2013**, *15*, 271–286. [[CrossRef](#)] [[PubMed](#)]
61. Thakar, J.; Pathak, A.K.; Murphy, L.; Albert, R.; Cattadori, I.M. Network model of immune responses reveals key effectors to single and co-infection dynamics by a respiratory bacterium and a gastrointestinal helminth. *PLoS Comput. Biol.* **2012**, *8*, e1002345. [[CrossRef](#)] [[PubMed](#)]
62. Enciso, J.; Mayani, H.; Mendoza, L.; Pelayo, R. Modeling the pro-inflammatory tumor microenvironment in acute lymphoblastic leukemia predicts a breakdown of hematopoietic-mesenchymal communication networks. *Front. Physiol.* **2016**, *7*, 349. [[CrossRef](#)]
63. Ding, S.; Wang, W. Recipes and mechanisms of cellular reprogramming: A case study on budding yeast *Saccharomyces cerevisiae*. *BMC Syst. Biol.* **2011**, *5*, 50. [[CrossRef](#)]
64. Li, F.; Long, T.; Lu, Y.; Ouyang, Q.; Tang, C. The yeast cell-cycle network is robustly designed. *Proc. Natl. Acad. Sci. USA* **2004**, *101*, 4781–4786. [[CrossRef](#)]
65. Huitzil, S.; Sandoval-Motta, S.; Frank, A.; Aldana, M. Modeling the Role of the Microbiome in Evolution. *Front. Physiol.* **2018**, *9*, 1836. [[CrossRef](#)]
66. Kim, H. The Role of Criticality of Gene Regulatory Networks on Emergent Properties of Biological Systems. Ph.D. Thesis, Binghamton University, Binghamton, NY, USA, 10 May 2018.
67. Santamaría-Bonfil, G.; Gershenson, C.; Fernández, N. A Package for Measuring emergence, Self-organization, and Complexity Based on Shannon entropy. *Front. Robot. AI* **2017**, *4*, 10. [[CrossRef](#)]
68. Fernández, N.; Maldonado, C.; Gershenson, C. Information measures of complexity, emergence, self-organization, homeostasis, and autopoiesis. In *Guided Self-Organization: Inception*, 1st ed.; Prokopenko, M., Ed.; Springer: Berlin/Heidelberg, Germany, 2014; pp. 19–51.
69. Gershenson, C.; Fernández, N. Complexity and information: Measuring emergence, self-organization, and homeostasis at multiple scales. *Complexity* **2012**, *18*, 29–44. [[CrossRef](#)]
70. Gershenson, C. The sigma profile: A formal tool to study organization and its evolution at multiple scales. *Complexity* **2011**, *16*, 37–44. [[CrossRef](#)]
71. Chawla, N.V.; Bowyer, K.W.; Hall, L.O.; Kegelmeyer, W.P. SMOTE: Synthetic minority over-sampling technique. *J. Artif. Intell. Res.* **2002**, *16*, 321–357. [[CrossRef](#)]

72. He, H.; Bai, Y.; Garcia, E.A.; Li, S. ADASYN: Adaptive synthetic sampling approach for imbalanced learning. In Proceedings of the 2008 IEEE International Joint Conference on Neural Networks (IEEE World Congress on Computational Intelligence), Hong Kong, China, 1–8 June 2008; IEEE: Piscataway Township, NJ, USA, 2008; pp. 1322–1328.
73. Krawitz, P.; Shmulevich, I. Basin entropy in Boolean network ensembles. *Phys. Rev. Lett.* **2007**, *98*, 158701. [[CrossRef](#)] [[PubMed](#)]
74. Saito, T.; Rehmsmeier, M. The precision-recall plot is more informative than the ROC plot when evaluating binary classifiers on imbalanced datasets. *PLoS ONE* **2015**, *10*, e0118432. [[CrossRef](#)] [[PubMed](#)]
75. Dubrova, E.; Teslenko, M. A SAT-based algorithm for finding attractors in synchronous boolean networks. *IEEE/ACM Trans. Comput. Biol. Bioinform.* **2011**, *8*, 1393–1399. [[CrossRef](#)]



© 2020 by the authors. Licensee MDPI, Basel, Switzerland. This article is an open access article distributed under the terms and conditions of the Creative Commons Attribution (CC BY) license (<http://creativecommons.org/licenses/by/4.0/>).